HHS Public Access

Author manuscript

Cell Rep. Author manuscript; available in PMC 2024 June 06.

Published in final edited form as:

Cell Rep. 2024 May 28; 43(5): 114123. doi:10.1016/j.celrep.2024.114123.

Oligodendrocyte-derived laminin-γ1 regulates the blood-brain barrier and CNS myelination in mice

Minkyung Kang[1], **Yao Yao**[1,2,*]

[1]Department of Molecular Pharmacology and Physiology, Morsani College of Medicine, University of South Florida, Tampa, FL, 33612, USA

[2]Lead contact

SUMMARY

Although oligodendrocytes (OLs) synthesize laminin-γ1, the most widely used γ subunit, its functional significance in the CNS remains unknown. To answer this important question, we generated a conditional knockout mouse line with laminin-γ1-deficiency in OL lineage cells (γ1-OKO). γ1-OKO mice exhibit weakness/paralysis and die by P33. Additionally, they develop blood-brain barrier (BBB) disruption in the cortex and striatum. Subsequent studies reveal decreased Mfsd2a expression and increased endothelial caveolae vesicles, but unaltered tight junction protein expression and tight junction ultrastructure, indicating a transcellular rather than paracellular mechanism of BBB breakdown. Furthermore, significantly reduced OL lineage cells, OL precursor cells (OPCs), proliferating OPCs, and mature-OLs are observed in γ1-OKO brains in a region-specific manner. Consistent with this finding, various defects in myelination are detected in γ1-OKO brains at biochemical and ultrastructural levels. Overall, these results highlight important roles of OL-derived laminin-γ1 in BBB maintenance and OL biology (proliferation, differentiation, and myelination).

Graphical Abstract

*Corresponding Author: Yao Yao, PhD, FAHA, Molecular Pharmacology and Physiology, Morsani College of Medicine, University of South Florida, 12901 Bruce B. Downs Blvd., MDC 8, Tampa, FL 33612, USA, yao7@usf.edu.

Author Contributions

Y.Y. conceived the project. M.K. and Y.Y. designed experiments. M.K. performed experiments and wrote the manuscript. Y.Y. revised the manuscript.

Declaration of interests

The authors declare no competing interests.

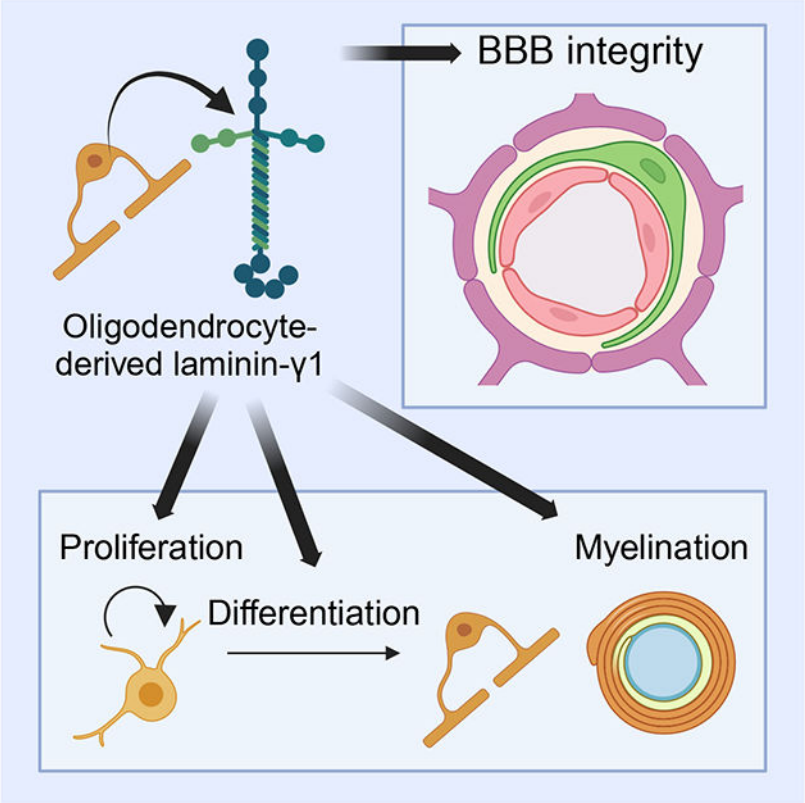

Keywords

Laminin; oligodendrocyte; blood-brain barrier; myelination

INTRODUCTION

Laminin, a major component of the extracellular matrix (ECM), is a heterotrimeric protein containing one α chain, one β chain, and one γ chain. Due to genetic variance, five α, four β, and three γ chains have been identified in mammals, which generates many different laminin isoforms. In the CNS, vessel-associated cells, including endothelial cells and mural cells (pericytes and vascular smooth muscle cells) as well as astrocytes, synthesize and deposit various laminin isoforms to the basal lamina (BL), which regulate blood-brain barrier (BBB) integrity under both physiological and pathological conditions.[1,2] For example, astrocytes express laminin-α2β1γ1 (−211), which maintains BBB integrity via regulating pericyte differentiation.[3] Deletion of endothelial cell-derived laminin α5 alone fails to affect BBB integrity under homeostatic conditions, but exacerbates BBB damage in an intracerebral hemorrhage model.[4] Pericytes mainly make laminin-α2/α4/α5 and -γ1.[5–7] Loss of laminin-γ1 in mural cells causes BBB breakdown in an age-dependent manner,[7] whereas ablation of laminin α5 in mural cells fails to affect BBB integrity under homeostatic conditions but ameliorates BBB damage in an ischemia-reperfusion model.[8] Currently, whether non-vessel-associated cells, such as oligodendrocytes (OLs), synthesize laminin remains largely unknown.

OLs are the only myelinating cells in the CNS. Depending on their morphology and markers, oligodendrocytes are categorized into oligodendrocyte precursor cells (OPCs), pre-myelinating oligodendrocytes (pre-OLs), and mature oligodendrocytes (mature-OLs). Mature-OLs wrap axons with myelin sheaths, enabling efficient action potential transduction. Other than myelination, there is also evidence suggesting that OLs may be involved in BBB regulation. For example, both OPCs[9] and mature-OLs[10] have been found to make direct contact with blood vessels. In addition, aberrant clustering of OPCs at the BBB triggers BBB disruption and CNS inflammation.[11] How exactly OLs modulate BBB integrity, however, remains unknown.

Recent studies show that OLs, like vascular cells, can also make laminin. For instance, RNA-sequencing studies demonstrate that OL lineage cells express various laminin chains, including laminin-γ1, at mRNA level.[6,12,13] Furthermore, a secretome analysis reports expression of many laminin chains, including laminin-γ1, at protein level in pre-OLs.[14] What is the function of OL-derived laminin? Is it necessary for BBB integrity? Does it regulate OL biology, including proliferation, differentiation, and myelination?

To answer these important questions and investigate the functional significance of OL-derived laminin, we generated mutant mice with laminin-γ1 deletion in OL lineage cells. Our results show that OL-derived laminin is crucial for BBB maintenance and actively regulates oligodendrocyte proliferation, differentiation, and myelination *in vivo*.

RESULTS

Efficient deletion of *Lamc1* in OL lineage cells in γ1-OKO mice

To investigate the function of OL-derived laminin-γ1, we generated OL-specific laminin-γ1 knockout mice (γ1-OKO) using Sox10-Cre line, which specifically labels OL lineage cells in the CNS.[6,15,16] Since laminin-γ1 is located in the BL exclusively and other cells also deposit laminin-γ1 to the BL,[1,2] it is impossible to determine the cellular source of laminin-γ1 by immunohistochemistry (IHC). Instead, we validated the knockout efficiency by *in situ* hybridization (RNAscope). We found that approximately 36-41% of OL lineage cells express *Lamc1* transcript in the cortex, corpus callosum, and striatum of control mice (Figure 1). To determine if *Lamc1* is expressed exclusively in a specific population, we further examined *Lamc1* expression in OPCs and mature-OLs. Our analyses revealed both $Lamc1^{+}$ and $Lamc1^{-}$ cells in $Pdgfra^{+}Sox10^{+}$ OPCs and $Mbp^{+}Sox10^{+}$ mature-OLs (Figure S1A and S1B). These results suggest that *Lamc1* is synthesized by both populations of OLs, and that not all cells in each population express *Lamc1*, possibly reflecting different subpopulations. In sharp contrast, less than 6% of OL lineage cells expressed *Lamc1* transcript in all three brain regions in γ1-OKO mice (Figure 1), indicating efficient deletion of *Lamc1* in OL lineage cells in γ1-OKO mice. Next, we also examined laminin-γ1 expression in primary OLs isolated from control and γ1-OKO brains. Although detected in control OLs, laminin-γ1 was absent in γ1-OKO OLs (Figure S1C and S1D), again suggesting successful ablation of *Lamc1* in OL lineage cells in γ1-OKO mice.

Since Sox10 marks early neural crest cells,[17–20], which may differentiate into brain mural cells (pericytes and smooth muscle cells),[21] we further examined if laminin-γ1 expression

was affected in these cells. Our IHC/ISH analyses showed that *Lamc1* mRNA was detected in PDGFRβ$^+$ pericytes in both control and γ1-OKO brains (Figure S2A). Quantification revealed comparable numbers of *Lamc1*-expressing pericytes in all three brain regions (cortex, corpus callosum, and striatum) between control and γ1-OKO mice (Figure S2B–S2D). Similarly, *Lamc1* mRNA was also detected in PDGFRβ$^+$SMA$^+$ smooth muscle cells (Figure S2E), and no differences in the numbers of *Lamc1*-expressing smooth muscle cells were found in control and γ1-OKO brains (Figure S2F–S2H). These results suggest that mural cell-derived *Lamc1* is unaffected in γ1-OKO mice.

γ1-OKO mice exhibit muscle weakness and severe BBB disruption

γ1-OKO mice were born at the expected Mendelian ratio and appeared normal at birth. However, the mutants were noticeably smaller compared to their littermate controls by postnatal day (P) 8 (Figure 2A). By P28, the mutants developed near-complete hindlimb paralysis and tremor (Figure 2B). In addition, the mutants showed reduced survival: all mutants died by P33 (Figure 2C).

To investigate whether OL-derived laminin, like vascular cell-derived laminin, also regulates BBB integrity, we first performed *in vivo* BBB permeability assay. At P1, no hemoglobin was detected in control or γ1-OKO brains (Figure 2D–2F), indicating that BBB formation was not affected in γ1-OKO mice. Interestingly, γ1-OKO mice exhibited significantly higher levels of hemoglobin in both cortex and striatum at P8 (Figure 2G–2I) and P28 (Figure 2J–2L), suggesting an indispensable role of OL-derived laminin-γ1 in BBB maintenance. Subsequent analysis revealed that BBB breakdown mainly occurred in α-smooth muscle actin (SMA)$^-$ capillaries, although leakage from SMA$^+$ arterioles/arteries were occasionally observed (Figure S3A). Consistent with the hemoglobin data, retro-orbitally injected exogenous tracer showed similar results. Specifically, substantially more 4kD-FITC-Dextran was detected in the brain parenchyma of γ1-OKO mice compared to that of controls at P15-17 (Figure S3B), again indicating a crucial role of OL-derived laminin-γ1 in BBB maintenance.

Next, we performed angioarchitecture analysis in both cortex and striatum of γ1-OKO mice at P15-17. No differences in explant area, vessels area, vessels percentage area, total number of junctions, junction density, total vessel length, average vessel length, total number of end points, and average lacunarity were detected between control and γ1-OKO mice (Figure S4). These results suggest that BBB breakdown in γ1-OKO mice is not caused by vascular malformation.

Accumulating evidence supports an important role of Wnt/β-catenin signaling pathway in BBB maturation and function.[5,22–24] To investigate if abnormal Wnt/β-catenin signaling contributes to BBB disruption in γ1-OKO mice, we examined the expression of Lef1 and Sox17, two Wnt/β-catenin target genes, in blood vessels (Figure S5). Our analyses revealed comparable Lef1$^+$ cell number and Lef1 fluorescent intensity in the cortex (Figure S5B and S5D), corpus collosum (Figure S5G and S5I), and striatum (Figure S5L and S5N) between control and γ1-OKO mice. Similarly, no differences in Sox17$^+$ cell number and Sox17 fluorescent intensity were found in control and γ1-OKO brains (Figure S5C, S5E, S5H, S5J,

S5M, and S5O). These results suggest that BBB breakdown in γ1-OKO mice is not caused by aberrant Wnt/β-catenin signaling.

Tight junction is intact in γ1-OKO mice

BBB breakdown may be mediated by two different mechanisms. One is the paracellular mechanism, where tight junction is damaged, allowing molecules to pass through gaps between two adjacent endothelial cells.[25,26] The other is the transcellular mechanism, where increased transcytosis facilitates movement of molecules through endothelial cells.[25,27] To investigate if the paracellular mechanism is affected in γ1-OKO mice, we examined the expression of ZO-1 and claudin-5, two major tight junction proteins. In both cortex and striatum, IHC failed to detect any changes in ZO-1 intensity (Figure 3A, 3B, 3F, 3J, 3K, and 3O) or coverage (Figure 3A, 3D, 3H, 3J, 3M, and 3Q) between control and γ1-OKO mice at P15-17 (Figure 3A–3I) or P28 (Figure 3J–3R). Like ZO-1, comparable claudin-5 intensity (Figure 3A, 3C, 3G, 3J, 3L, and 3P) and coverage (Figure 3A, 3E, 3I, 3J, 3N, and 3R) were observed in control and γ1-OKO brains at both ages. Similarly, western blot analysis revealed no differences in ZO-1 (Figure 3S–3V) and claudin-5 (Figure 3W–3Z) expression in control and γ1-OKO brains. Consistent with these results, TEM analysis revealed intact tight junction structure in both control and γ1-OKO mice at P15-17 (Figure 3AA). More importantly, we further demonstrated that tight junctions prevented the leakage of HRP in both control and γ1-OKO mice (Figure 3AB). Together, these findings highlight a dispensable role of OL-derived laminin-γ1 in tight junction protein expression and tight junction structure & function.

Transcellular transport is increased in γ1-OKO mice

To determine if the transcellular mechanism contributes to BBB disruption in γ1-OKO mice, we examined the expression of major facilitator superfamily domain containing 2a (Mfsd2a), which negatively regulates transcytosis in endothelial cells.[28] Significantly decreased Mfsd2a intensity (Figure 4A–4C) and coverage on capillaries (Figure 4D and 4E) were found in both cortex and striatum of γ1-OKO mice at P28 compared to age-matched controls. Similarly, western blot analysis revealed substantially lower Mfsd2a levels in both cortex (Figure 4F and 4H) and striatum (Figure 4G and 4I) of γ1-OKO mice, indicating elevated endothelial transcellular transport. Consistent with these findings, TEM analysis revealed significantly more HRP-vesicles in endothelial cells from γ1-OKO brains at P15-17 (Figure 4J and 4K). These findings suggest that OL-derived laminin-γ1 maintains BBB integrity by inhibiting transcellular transport.

OL lineage cells are decreased in γ1-OKO mice

We investigated potential roles of OL-derived laminin-γ1 in OL biology. First, we examined if the number of OL lineage cells, including OPCs, pre-OLs, and mature-OLs, is affected in γ1-OKO mice by IHC against OL lineage marker Olig2 (Figure S6A). To enable a comprehensive and dynamic review, analysis was performed in three different brain regions (cortex, corpus callosum, and striatum) and at four different time points (P1, P8, P15-17, and P28). Control and γ1-OKO mice showed comparable OL lineage cells in all three brain regions at P1 (Figure S6B–S6D). In contrast, the numbers of OL lineage cells significantly decreased in γ1-OKO mice compared to the controls in all three brain regions at P8 (Figure

S6E–S6G). Similar changes were observed in γ1-OKO brains at P15-17, but statistical significance was only achieved in the cortex and the striatum (Figure S6H–S6J). By P28, substantially reduced OL lineage cell numbers were again detected in all three brain regions in γ1-OKO mice (Figure S6K–S6M). These results indicate that OL-derived laminin-γ1 positively regulates OL lineage cell number starting from P8.

OPCs and proliferating OPCs are decreased in γ1-OKO mice

We then asked if OL-derived laminin-γ1 differentially regulates different populations of OL lineage cells. First, we examined the numbers of OPCs in control and γ1-OKO mice by co-staining of Olig2 and OPC marker, PDGFRα (Figure 5A). Although no differences in $Olig2^{+}PDGFR\alpha^{+}$ OPC numbers were detected in control and γ1-OKO brains at P1 (Figure 5B–5D), γ1-OKO mice showed significantly reduced OPC numbers in all three brain regions (cortex, corpus collosum, and striatum) at P8 (Figure 5E–5G). Interestingly, diminished OPC numbers were only observed in the cortex but not corpus callosum or striatum in γ1-OKO mice at P15-17 (Figure 5H–5J). By P28, decreased OPC numbers were found in both cortex and corpus callosum but not striatum in γ1-OKO mice (Figure 5K–5M). These results suggest that OL-derived laminin-γ1 positively regulates OPC number in a region-specific manner.

OPCs are highly proliferative in the CNS throughout life.[29] To further determine if loss of OL-derived laminin-γ1 affects OPC numbers via regulating their proliferation, we performed triple staining against Olig2, PDGFRα, and Ki67 (Figure S7A). At P1 and P8, no significant differences in the numbers of proliferating OPCs ($Olig2^{+}PDGFR\alpha^{+}Ki67^{+}$ cells) were detected in control and γ1-OKO brains (Figure S7B–S7G). By P15-17 (Figure S7H–S7J) and P28 (Figure S7K–S7M), however, significantly reduced numbers of proliferating OPCs were observed in all three brain regions (cortex, corpus callosum, and striatum) in γ1-OKO mice compared to the controls. These findings suggest that OL-derived laminin-γ1 positively regulates OPC proliferation starting from P15-17.

Mature-OLs are decreased in γ1-OKO mice

Next, we examined the numbers of mature-OLs in γ1-OKO brains at P28, a time point when mature-OLs become abundant in the CNS.[30] To do this, co-staining of Sox10 (OL lineage marker) and CC1 (mature-OL marker) was performed. IHC analysis revealed lower numbers of $Sox10^{+}CC1^{+}$ mature-OLs in all three brain regions (cortex, corpus collosum, and striatum) in γ1-OKO mice compared to the controls (Figure 6), highlighting an important role of OL-derived laminin-γ1 in OL maturation. Given the unaltered OPC number (Figure 5M) and decreased OL lineage cell number (Figure S6M) in the striatum of γ1-OKO mice at P28, the reduced mature-OLs in this region is likely due to delayed differentiation of OPCs. Together, these findings suggest that OL-derived laminin-γ1 may regulate OPC differentiation.

Myelination is impaired in γ1-OKO mice

One major function of mature-OLs is to myelinate axons. Thus, we further investigated if myelination is affected in γ1-OKO brains. Quantitative western blot revealed substantially lower levels of myelin basic protein (MBP), a major myelin protein, in all three brain

regions in γ1-OKO mice at P15-17 (Figure 7A–7F), highlighting an essential role of OL-derived laminin-γ1 in myelination. To further analyze myelination defects, we performed TEM analysis using corpus callosum samples from control and γ1-OKO mice at P15-17. Overall, γ1-OKO brains exhibited reduced density of myelinated fibers compared to the controls (Figure 7G). In addition, thinner compact myelin sheaths and disturbed circularity of myelinated fibers were observed in γ1-OKO brains compared to the controls (Figure 7G). To quantitatively measure the thinning of compact myelin sheaths, g-ratio was calculated by measuring diameters of axon, myelinated fiber, and inner tongue (Figure 7H). γ1-OKO mice showed significantly increased g-ratio compared to the controls (Figure 7I), indicating thinning of compact myelin sheaths. When plotted against axon caliber, g-ratio demonstrated an upshift across axons of all calibers (0.3-3 μm) in γ1-OKO mice (Figure 7J), suggesting that the defect (thinning of compact myelin sheaths) is independent of axon size. In addition, we also found significantly decreased density of myelinated fibers in γ1-OKO brains (Figure 7K). The mean gray value (MGV) of compact myelin sheaths was also decreased in γ1-OKO brains, although this change was not statistically significant (Figure 7L). Finally, morphological changes of myelinated fibers were measured and categorized into four groups: myelin sheath splitting, inner tongue enlargement, myelin outfolding, and myelin debris (Figure 7M). We found significantly increased myelin sheath splitting (Figure 7N), inner tongue area (Figure 7O), and myelin outfolding (Figure 7P) in γ1-OKO brains compared to the controls. Although increased myelin debris was also found in γ1-OKO brains, this change did not reach statistical significance (Figure 7Q). These results indicate structural abnormalities of myelinated fibers in γ1-OKO mice. Together, these findings strongly suggest that OL-derived laminin-γ1 actively regulates myelination.

DISCUSSION

In this study, we investigated the function of OL-derived laminin-γ1 in BBB maintenance and OL biology using mutants with laminin-γ1 deficiency in OL lineage cells (γ1-OKO). Our results show that OL-derived laminin-γ1 actively: (1) maintains BBB integrity via the transcellular rather than paracellular mechanism, and (2) regulates OL proliferation, differentiation, and myelination in a region-specific manner. This loss-of-function study systemically characterizes the functional significance of OL-derived laminin-γ1 *in vivo*.

Mounting evidence supports that OPCs and OLs contribute to the barrier function of the BBB via multiple mechanisms. For example, using both *in vitro* and *in vivo* approaches, it has been shown that OPCs support BBB integrity via TGF-β signaling.[31] Another study finds that OPCs up-regulate BBB function through a PDGFRα-dependent manner, whereas OLs do so via PDGFRα-independent mechanisms.[32] In addition, aberrant oligodendroglial-vascular interactions have been found to disrupt BBB integrity and the underlying mechanism involves abnormal Wnt signaling.[11] Similarly, OPC transplantation has been demonstrated to enhance BBB function after cerebral ischemia.[33] Furthermore, BBB defect has been reported in a mouse model of neurofibromatosis, where nitric oxide production is dysregulated in OLs,[34] suggesting that OLs may regulate BBB integrity via nitric oxide signaling. In this study, we report a previously unidentified mechanism for this BBB-protective effect of OLs. Specifically, we find that OLs may regulate BBB integrity via laminin signaling.

This report clearly shows that non-vascular cell-derived laminin, like vascular cell-derived laminin, contributes to BBB maintenance. Vascular cells, including endothelial cells, pericytes and astrocytes, can synthesize and deposit laminin directly to the BL due to their close anatomical proximity.[1,2] OLs, on the other hand, are not a major component of the BBB and do not seem to contact the BL directly in normal adult brains. How does OL-derived laminin reach the BL and support BBB integrity? One possibility is that OL lineage cells may deposit laminin to the BL at a specific developmental stage when they make physical interactions with cerebral vasculature. It has been shown that OPCs use the vasculature as the substrate for migration during development.[35] Similarly, an immuno-electron microscopy study finds that OPCs interact with cerebral endothelial cells via BL in neonatal mouse brains.[9] Another possibility is that subpopulations of OLs may have direct contact with the BL in normal adult brains. A recent study reports that, in adult mice, one out of six mature-OLs make direct contact with the BL of the BBB.[10] Together, these results support the possibility that OL-derived laminin contributes to the maintenance of BBB integrity. Several important questions, however, should be addressed in future research. For example, whether OL-derived laminin is deposited and incorporated into the BL needs to be determined. Given that only 36-41% of OL lineage cells expressed *Lamc1* in the CNS (Fig. 1), it is important to distinguish $Lamc1^{+}$ and $Lamc1^{-}$ subpopulations. It would be also interesting to characterize the molecular signature and functional significance of $Lamc1^{+}$ and $Lamc1^{-}$ subpopulations.

Another key finding of this study is that OL-derived laminin-γ1 actively regulates their proliferation, differentiation, and myelination. Although there are reports showing that laminin participates in the regulation of OL biology (survival, proliferation, differentiation, and maturation),[36] these studies have two caveats. First, most if not all previous studies were performed *in vitro* using cultured OLs. No *in vivo* studies are available currently. Next, none of previous studies used OL-derived laminin. Instead, mouse Engelbreth-Holm-Swarm (EHS) sarcoma-derived laminin was used. Since different cells make distinct laminin isoforms,[1,2,37] the function of OL-derived laminin remains unknown. Here, we provide *in vivo* evidence that OL-derived laminin-γ1 regulates their biology. In addition, we also investigated the roles of OL-derived laminin-γ1 in OL biology in a region/age-specific manner. What confers the region-specific effect, however, remains unclear. One possible explanation is compensation by laminin derived from other cells. A thorough understanding of laminin expression and function in the CNS will shed light on this important question.

Our *in situ* hybridization and/or IHC analyses suggest that Sox10-Cre specifically labels OL lineage cells without affecting mural cells in the CNS. This is consistent with previous reports showing high specificity of the Sox10-Cre (personal communication) and Sox10-$CreER^{T216}$ lines in OL lineage cells with minimal labeling of mural cells. In contrast, one fate-mapping study reported that $Sox10^{+}$ cells can differentiate into mural cells in the brain.[38] It should be noted, however, that this study did not use Sox10-Cre. Instead, a transgenic line expressing Cre under c-fos promoter and a Sox10 distal enhancer [39] was used and wrongly cited as Sox10-Cre. Different Cre lines may explain the distinct findings.

It is worth noting that Sox10-Cre also labels Schwann cells in the periphery[40] in addition to OL lineage cells in the CNS.[6,15,16] Thus, laminin-γ1 is ablated in both OLs and Schwann

cells in γ1-OKO mice. However, given the different locations of Schwann cells and OLs, we believe the CNS-specific phenotype (BBB disruption and defects in OL biology) is more likely caused by loss of OL-derived laminin-γ1, whereas the peripheral phenotype (muscle weakness and paralysis) is possibly due to loss of laminin-γ1 in both OLs and Schwann cells. Consistent with this hypothesis, mice with laminin-γ1 deficiency in Schwann cells have intact BBB integrity[41] and exhibit a milder peripheral phenotype compared to γ1-OKO mice.[42] Specifically, these mutants start to show hindlimb weakness at ~4 weeks and become near-complete paralysis by 3 months,[42] whereas γ1-OKO mice show early onset and rapid progression of muscle weakness and all die by P33. These findings underscore an essential role of OL- rather than Schwann cell-derived laminin-γ1 in BBB maintenance and OL biology.

Limitations of the study

One limitation of this study is that the causal relationship between BBB disruption and OL defects in γ1-OKO mice remains unclear. One possibility is that loss of laminin-γ1 in OL lineage cells affects their differentiation/maturation initially, which has a secondary effect on BBB integrity. An alternative possibility is that loss of laminin-γ1 in OL lineage cells damages BBB integrity initially, which affects OL differentiation/maturation secondarily. A third possibility is that BBB breakdown and OL defects are two independent events. In this study, we performed analyses at four different time points (P1, P8, P15-P17, and P28) with the hope of determining the temporal profiles of BBB disruption and OL defects. However, this approach failed since neither defect was observed at P1 and both defects were detected at P8. This important question will be addressed in future research.

Another limitation of this study is that the specific laminin isoforms produced by OLs remain unknown. Previous RNA-sequencing and secretome analyses revealed expression of various laminin chains in OLs,[6,12–14] indicating that OLs may express multiple laminin isoforms. By ablating laminin-γ1, the most widely used γ chain in the CNS, we delete all γ1-containing laminin isoforms. Since different laminin isoforms may exert distinct functions,[1,2,37] it is important to determine the specific laminin isoforms expressed in OLs. Since different populations of OLs (OPCs, pre-OLs, and mature-OLs) may make distinct laminin isoforms, laminin expression in these populations should be characterized in future work. In addition, the receptors that mediate laminin signaling in OLs remain unknown. Future work should identify the receptors and possibly downstream signaling pathways in OLs, which will provide molecular targets with therapeutic potential in a variety of neurological disorders.

STAR★Methods

RESOURCE AVAILABILITY

Lead contact—Further information and requests for resources and reagents should be directed to and will be fulfilled by the lead contact, Yao Yao (yao7@usf.edu).

Materials availability—Materials will be shared upon request within the limits of the respective material transfer agreements.

Data and code availability

- Raw data from Figures 1–7 and Figures S1–S7 were deposited on Mendeley at https://digitalcommonsdata.usf.edu/datasets/jmszrtgd48/draft?a=14077a44-68de-4f5b-bcb7-40e5a304e4b3.
- This paper does not report original code.
- Any additional information required to reanalyze the data reported in this paper is available from the lead contact upon request.

EXPERIMENTAL MODEL AND SUBJECT DETAILS

Mouse generation

Laminin $\gamma1^{flox/flox}$ mice and Sox10-Cre^{+} mice were crossed to generate Laminin $\gamma1^{flox/flox}$;Sox10-Cre^{+} (γ1-OKO) mice. Heterozygotes (Laminin $\gamma1^{flox/+}$;Sox10-Cre^{+}) were indistinguishable from Laminin $\gamma1^{flox/flox}$ or Laminin $\gamma1^{flox/+}$ littermates. Thus, these mice were all used as controls. Mice were analyzed at four ages: P1, P8, P15-17, and P28. Both sexes were included in our analyses.

Mouse maintenance

All mice were maintained in the animal facility at the University of South Florida. They were kept in ventilated cages with free access to water and food, under specific pathogen-free conditions and 12 h/12 h light/dark cycle. All procedures were in compliance with the NIH guide and approved by the Institutional Animal Care and Use Committee (IACUC).

METHOD DETAILS

RNAscope *in situ* hybridization

RNAscope multiplex fluorescent reagent kit V2 (Advanced Cell Diagnostics, 323100) was used on 20 μm-thick sections, following the manufacturer's instructions. The specific probes used in this study are: *Lamc1* (Cat #: 517451), *Sox10* (Cat #: 435931-C3), *Pdgfra* (Cat #: 480661-C2), and *Mbp* (Cat #: 451491-C21).

In situ hybridization and immunohistochemistry (IHC/ISH) co-staining was performed as described previously.[43] Briefly, *in situ* hybridization was performed following the manufacturer's instructions until the final HRP blocking step. Then the slides were washed in RNAscope Wash Buffer (4 times, 5 minutes each), PBS (3 times, 5 minutes each), and 0.5% PBST (2 times, 5 minutes each). The slides were incubated in blocking buffer containing 10% donkey serum and 0.5% fish skin gelatin in 0.5% PBST for 1.5 hours at room temperature. Primary antibodies were made in the same blocking buffer for overnight incubation. Next day, the slides were washed in 0.5% PBST (3 times, 5 minutes each), followed by incubation in secondary antibodies for 2 hours at room temperature. Next, the slides were washed with 0.5% PBST (2 times, 5 minutes each), 0.1M PB buffer (2 times, 5 minutes each), and distilled water before mounted with Fluoromount-G with DAPI.

Immunohistochemistry (IHC)

Brains were cut into 20 μm-thick sections with a Cryostat (CryoStar NX50, Thermo Scientific, US) and mounted onto positively charged glass slides (Superfrost™ Plus). Brain sections were fixed in 4% PFA for 20 minutes and washed 3 times with PBS. Next, blocking buffer (1% BSA in PBS containing 0.3% normal donkey serum and 0.3% Triton X-100) was applied on the sections for 90 minutes at room temperature, followed by incubation with primary antibodies overnight at room temperature. The following primary antibodies were used: anti-hemoglobin (Cloud-Clone, PAB409Mu01, 1:500), anti-podocalyxin (R&D, AF1556, 1:400), anti-ZO1 (ThermoFisher, 61-7300, 1:500), anti-claudin5 (Invitrogen, 35-2500, 1:200), anti-Mfsd2a (a generous gift from Dr. Chenghua Gu, 1:200), anti-Olig2 (Novus, NBP1-28667, 1:500), anti-PDGFRα (R&D, AF2535, 1:400), anti-Sox10 (R&D, AF2864-SP, 1:300), anti-CC1 (Calbiochem, OP80, 1:300), anti-MBP (BioRad, MCA409S, 1:200), anti-PDGFRβ (Cell Signaling, 3169S, 1:400), anti-SMA-Cy3 (Sigma, C6198, 1:400), anti-SMA-FITC (Sigma, F3777, 1:500), anti-Lef1 (Cell Signaling, 2230S, 1:500), anti-Sox17 (R&D, AF1924, 1:300), anti-CD31 (BD, 553370, 1:100), and anti-Ki67 (GeneTex, GTX16667, 1:400). After extensive wash in PBS, the sections were incubated with appropriate secondary antibodies for 90 minutes at room temperature. The sections were washed again with PBS and mounted with Fluoromount-G with DAPI. For OPC proliferation analysis, anti-Olig2 (Millipore, MABN50, 1:200) and M.O.M.™ Kit (Vector Laboratories, Inc., FMK-2201) were used following the manufacturer's instructions. Images were obtained using Nikon Eclipse Ti, Nikon Eclipse Ni, and Keyence BZ-X710 microscopes. Image processing was done in ImageJ (NIH) and Adobe Photoshop.

Primary OPC culture

Primary OPCs were isolated by MACS as described previously.[44,45] Briefly, brains were collected from control and γ1-OKO mice at P6 and digested in papain solution (Worthington Biochemical Corporation, LK003178) containing DNase I (5mg/ml, Worthington Biochemical Corporation, LS002007) for 45 minutes at 37°C. Next, the solutions were filtered through 100 um cell strainers, followed by centrifugation at 1500 rpm for 7 minutes. The pellets were resuspended in resuspension solution containing albumin-ovomucoid inhibitor (10mg/ml ovomucoid and 10mg/ml BSA, Worthington Biochemical Corporation, LK003182) and DNase I. A discontinuous density gradient was prepared by carefully adding albumin-ovomucoid inhibitor solution to the bottom and cell suspension on top. After centrifugation at 590 rpm for 7 minutes, the supernatant was discarded and the pellet was resuspended in MACS buffer (0.5% BSA in DPBS). After wash in MACS buffer, the cells were incubated with FcR blocking reagent (Ultra-LEAF™ Purified anti-mouse CD16/32 antibody, Biolegend, 101330) for 10 minutes on ice. Next, anti-O4 MicroBeads (Miltenyi Biotec, 130-096-670) was added to and incubated with the cells for 30 minutes on ice. After extensive wash, cell suspension was added to a LS column (Miltenyi Biotec, 130-042-401) placed on a MACS separator (Miltenyi Biotec, 130-042-501). $O4^+$ cells were then eluted with elution buffer. To ensure high purity, two LS columns were used. Eluted cells were immediately resuspended in OPC medium (DMEM with 4mM L-glutamine and 1mM sodium pyruvate, 0.1% BSA, 50μg/ml apo-transferrin, 5μg/ml insulin, 30nM sodium selenite, 10nM D-biotin, 10nM hydrocortisone, 10ng/ml PDGF-AA, and 10ng/ml b-FGF).

The cells were seeded onto PDL-coated coverslips in 24-well plates at the density of $2x10^4$/cm^2. The cells were cultured for 8 days with half medium change every other day.

Immunocytochemistry (ICC)

ICC was performed following standard protocol. Briefly, cells grown on coverslips were washed with DPBS, fixed with 4% PFA for 20 minutes, and washed with PBS for 3 times 5 minutes each. After incubation in blocking buffer (1% BSA in PBS containing 0.3% normal donkey serum and 0.3% Triton X-100) for 90 minutes, the cells were incubated with laminin-γ1 (NeoMarkers, RT-795-P, 1:100) antibody overnight at 4°C. Next day, the cells were washed with PBS (3 times, 5 minutes each) and incubated with Alexa Fluor-488 conjugated donkey anti-rat antibody (Invitrogen, A21208, 1:400) for 90 minutes at room temperature. After extensive wash, the cells were mounted with Fluoromount-G with DAPI.

BBB permeability assay

4kD FITC-Dextran (Sigma, FD4, 25 mg/ml in sterile saline, 2.5 μl/g of body weight) was injected retro-orbitally into mice. After 6 hours of circulation, mice were transcardially perfused with PBS and the brains was carefully dissected out. The brains were cut in half and one hemisphere was collected in a microcentrifuge tube with 800 μl of sterile saline. Then, the tissue was homogenized by sonication, followed by centrifugation at 15,000 rpm for 20 minutes. The supernatant was collected in a fresh tube, and 100 μl of the supernatant was added into a well of 96-well plate. The plate was read at 485/528 nm in a plate reader. Each sample was measured in triplicates from which an average value was obtained. 5-6 animals per group were used for quantification.

Brain angioarchitecture analysis

Angiotool (National Cancer Institute, US), an automated software to analyze angioarchitecture,[46] was used to analyze the brain angioarchitecture of control and γ1-OKO mice. Briefly, podocalyxin staining was done to visualize all blood vessels. After uploading images to the software, settings to remove small particles or fill holes were adjusted to selectively include the areas with podocalyxin signal. Next, explant area, vessel area, vessels percentage area, total number of junctions, junction density, total vessel length, average vessel length, total number of end points, and average lacunarity were analyzed in the software.

Transmission electron microscopy (TEM)

TEM was performed as described previously.[7,41,47–49] For TEM without HRP: P15-17 animals were perfused with PBS, followed by 4% PFA and 5% glutaraldehyde in 0.1 M Na-cacodylate (pH 7.4). The brains were dissected out and postfixed in 4% PFA and 5% glutaraldehyde in 0.1 M Na-cacodylate (pH 7.4) for an hour at room temperature, followed by 4% PFA in 0.1 M Na-cacodylate (pH 7.4) overnight at 4 °C. The next day, 50 μm-thick sections were obtained using a vibratome and stained in 1% osmium tetroxide for an hour at 4 °C and 2% uranyl acetate for 30 minutes at 4 °C. The tissues were then dehydrated with alcohol and embedded in resin. Next, 50nm-thick ultra-thin sections were cut with a

microtome, stained with 2% uranyl acetate, and imaged under JEOL 1400 (JEOL) at 80.0 kV.

For HRP-TEM: mice were anesthetized and retro-orbitally injected with HRP Type II (Sigma, P8250-25KU, 10mg/20g of body weight). After 45 minutes, the brains were dissected out and fixed by immersion in 4% PFA with 5% glutaraldehyde in 0.1 M sodium cacodylate buffer for 1 hour at room temperature. The brains were then transferred to 4% PFA in 0.1 M sodium cacodylate buffer for 5 hours, followed by incubation in 0.1 M sodium cacodylate buffer overnight. Next, 50 μm-think free-floating sections were cut using a vibratome. After washed with 0.05 M Tris-HCl buffer (pH 7.6), the sections were incubated in 0.05 M Tris-HCl buffer containing 3, 3'-diaminobenzidine (DAB, 5mg/10ml) with 0.01% H_2O_2 for 45 minutes at room temperature. Then, the sections were washed with 0.1 M sodium cacodylate buffer and PB buffer. Next, the sections were incubated in 3% potassium ferrocyanide in 0.1 M PB buffer and equal volume of 4% aqueous osmium tetroxide (EMS) for an hour. After extensive wash in ddH_2O, the tissues were placed in thiocarbohydrazide solution (TCH, Ted Pella, filtered through 0.22 μm syringe) for 20 minutes. Tissues were then washed in ddH_2O and incubated in 2% osmium tetroxide in ddH_2O for 30 minutes. After extensive wash in ddH_2O and dehydration in alcohol, the tissues were embedded in resin. Next, 50nm-thick ultra-thin sections were cut with a microtome, stained with 2% uranyl acetate, and imaged under JEOL 1400 (JEOL) at 80.0 kV.

Western blotting

Samples were prepared by dissecting and homogenizing the cortex, corpus callosum, and striatum of P15-17 mice. BCA Protein Assay Kit (Pierce, 23227) was used to determine total protein concentration. Equal amount of proteins was loaded and separated in SDS-PAGE, which then was transferred onto PVDF membranes. The membranes were incubated with primary antibodies overnight at 4 °C, followed by appropriate secondary antibodies for 90 minutes at room temperature. The following primary antibodies were used: anti-ZO1 (ThermoFisher, 61-7300, 1:500), anti-claudin5 (Invitrogen, 35-2500, 1:500), anti-Mfsd2a (a generous gift from Dr. Chenghua Gu, 1:500), MBP (BioRad, MCA409S, 1:500), and β-actin (BD, 612657, 1:2000). The membranes were developed with Clarity Max™ Western ECL Substrate (Bio-Rad, 1705062) and imaged using ChemiDoc XRS+ imaging system (Bio-Rad). For quantification, integrated density values of MBP were obtained using ImageJ (NIH) and normalized to that of β-actin.

QUANTIFICATION AND STATISTICAL ANALYSIS

Image analyses

Hemoglobin leakage was quantified by measuring the MGV of an image on ImageJ (NIH). $Lef1^+$ and $Sox17^+$ cell numbers were quantified manually, and the numbers were normalized to the area of CD31 signal. Lef1 and Sox17 intensity was measured by obtaining integrated density values after selecting the signal areas using thresholding function on ImageJ (NIH). Again, the values were normalized to the area of CD31 signal. For Mfsd2a expression, thresholding was applied to select podocalyxin-positive vessel areas, and MGV was measured on ImageJ (NIH) within the selected areas. Then, MGV from the background was

obtained to be subtracted from the Mfsd2a MGV to eliminate the effect of high background signal. Mfsd2a coverage (%) was measured by dividing the area of Mfsd2a signal by that of podocalyxin signal. ZO-1 and claudin5 intensity was measured by obtaining MGV after selecting the areas with the signal using thresholding function on ImageJ (NIH). ZO-1 or claudin5 coverage (%) was measured by dividing the area with ZO-1 or claudin5 signal by the area of podocalyxin signal. The numbers of $Olig2^+$, $Olig2^+PDGFR\alpha^+$, $Sox10^+CC1^+$, and $Olig2^+PDGFR\alpha^+Ki67^+$ cells were counted manually. Since images of the corpus callosum include areas that are adjacent to the structure, the numbers of cells were normalized to the area of the corpus callosum. For quantifications, 3-6 random images per section, 5-8 sections per mouse, and 3-5 mice were used.

For ICC analysis, the numbers of laminin-$\gamma1^+$ cells were manually quantified and divided by the number of $DAPI^+$ cells. For quantification, 4-8 images per replicate and 4 biological replicates were used.

For RNAscope analyses, the percentages of *Lamc1*-expressing OL lineage cells (*Sox10*$^+$ cells), pericytes ($PDGFR\beta^+$ cells), and SMCs ($PDGFR\beta^+SMA^+$ cells) were manually calculated.

Endothelial caveolae vesicles were quantified by normalizing the number of caveolae vesicles in endothelial cells to endothelial area. At least 10 capillaries per brain were used for quantification. Corrected g-ratio was quantified using the following equation: (axon diameter)/[(myelinated fiber diameter)-{(axon + inner tongue diameter)-(axon diameter)}] as described previously.[50] All diameters were obtained from area measurements ($\text{Diameter} = 2\sqrt{Area/\pi}$). At least 150 myelinated axons per brain were analyzed. Myelinated axon density was quantified by counting the number of myelinated fibers per image. The MGV of compact myelin sheaths was obtained using ImageJ (NIH) by thresholding the compact myelin areas. Morphology analysis was done manually by counting the numbers of myelinated fibers with split sheaths, outfolding, and myelin debris (with no axon present at the center) as described previously.[50] The percentages of myelin sheath splitting, myelin outfolding, and myelin debris were calculated out of at least 150 myelinated fibers per brain. Inner tongue enlargement was analyzed by measuring the area of inner tongue of at least 150 myelinated fibers per brain.

Statistical analyses

GraphPad Prism 9 was used for all statistical analyses performed. For normally distributed measurements, unpaired Student's t-test was applied, whereas non-normally distributed measurements were analyzed by Mann-Whitney u-test. Significance was set at $p < 0.05$. Data were presented as mean ± SD.

Supplementary Material

Refer to Web version on PubMed Central for supplementary material.

Acknowledgments

This work was supported by National Institutes of Health grants (R01HL146574, RF1AG065345, R01NS134134, R21AG073862, and R21AG064422) to Y.Y.. We thank Dr. Chenghua Gu for providing Mfsd2a antibody. We also thank Amanda Garces for her help with TEM microscopy. Graphical Abstract was created with BioRender.com.

References

1. Nirwane A, and Yao Y (2022). Cell-specific expression and function of laminin at the neurovascular unit. J. Cereb. Blood Flow Metab. 42, 1979–1999. 10.1177/0271678X221113027. [PubMed: 35796497]
2. Nirwane A, and Yao Y (2019). Laminins and their receptors in the CNS. Biol. Rev. Camb. Philos. Soc 94, 283–306. 10.1111/brv.12454. [PubMed: 30073746]
3. Menezes MJ, McClenahan FK, Leiton CV, Aranmolate A, Shan X, and Colognato H (2014). The extracellular matrix protein laminin α2 regulates the maturation and function of the blood-brain barrier. J. Neurosci 34, 15260–15280. 10.1523/JNEUROSCI.3678-13.2014. [PubMed: 25392494]
4. Gautam J, Miner JH, and Yao Y (2019). Loss of Endothelial Laminin α5 Exacerbates Hemorrhagic Brain Injury. Transl. Stroke Res 10, 705–718. 10.1007/s12975-019-0688-5. [PubMed: 30693425]
5. Biswas S, Shahriar S, Giangreco NP, Arvanitis P, Winkler M, Tatonetti NP, Brunken WJ, Cutforth T, and Agalliu D (2022). Mural Wnt/beta-catenin signaling regulates Lama2 expression to promote neurovascular unit maturation. Development 149, dev200610. 10.1242/dev.200610. [PubMed: 36098369]
6. Vanlandewijck M, He L, Mae MA, Andrae J, Ando K, Del Gaudio F, Nahar K, Lebouvier T, Lavina B, Gouveia L, et al. (2018). A molecular atlas of cell types and zonation in the brain vasculature. Nature 554, 475–480. 10.1038/nature25739. [PubMed: 29443965]
7. Gautam J, Cao Y, and Yao Y (2020). Pericytic Laminin Maintains Blood-Brain Barrier Integrity in an Age-Dependent Manner. Transl. Stroke Res 11, 228–242. 10.1007/s12975-019-00709-8. [PubMed: 31292838]
8. Nirwane A, Johnson J, Nguyen B, Miner JH, and Yao Y (2019). Mural cell-derived laminin-α5 plays a detrimental role in ischemic stroke. Acta Neuropathol. Commun 7, 23. 10.1186/s40478-019-0676-8. [PubMed: 30777135]
9. Seo JH, Maki T, Maeda M, Miyamoto N, Liang AC, Hayakawa K, Pham LD, Suwa F, Taguchi A, Matsuyama T, et al. (2014). Oligodendrocyte precursor cells support blood-brain barrier integrity via TGF-β signaling. PLoS One 9, e103174. 10.1371/journal.pone.0103174. [PubMed: 25078775]
10. Palhol JSC, Balia M, Sánchez-Román Terán F, Labarchède M, Gontier E, and Battefeld A (2023). Direct association with the vascular basement membrane is a frequent feature of myelinating oligodendrocytes in the neocortex. Fluids Barriers CNS 20, 24. 10.1186/s12987-023-00425-4. [PubMed: 37013659]
11. Niu J, Tsai HH, Hoi KK, Huang N, Yu G, Kim K, Baranzini SE, Xiao L, Chan JR, and Fancy SPJ (2019). Aberrant oligodendroglial-vascular interactions disrupt the blood-brain barrier, triggering CNS inflammation. Nat. Neurosci 22, 709–718. 10.1038/s41593-019-0369-4. [PubMed: 30988524]
12. Zhang Y, Chen K, Sloan SA, Bennett ML, Scholze AR, O'Keeffe S, Phatnani HP, Guarnieri P, Caneda C, Ruderisch N, et al. (2014). An RNA-sequencing transcriptome and splicing database of glia, neurons, and vascular cells of the cerebral cortex. J. Neurosci 34, 11929–11947. 10.1523/JNEUROSCI.1860-14.2014. [PubMed: 25186741]
13. He L, Vanlandewijck M, Mäe MA, Andrae J, Ando K, Del Gaudio F, Nahar K, Lebouvier T, Laviña B, Gouveia L, et al. (2018). Single-cell RNA sequencing of mouse brain and lung vascular and vessel-associated cell types. Sci. Data 5, 180160. 10.1038/sdata.2018.160. [PubMed: 30129931]
14. Kim WK, Kim D, Cui J, Jang HH, Kim KS, Lee HJ, Kim SU, and Ahn SM (2014). Secretome analysis of human oligodendrocytes derived from neural stem cells. PloS One 9, e84292. 10.1371/journal.pone.0084292. [PubMed: 24392122]
15. Zhang S, Rasai A, Wang Y, Xu J, Bannerman P, Erol D, Tsegaye D, Wang A, Soulika A, Zhan X, and Guo F (2018). The Stem Cell Factor Sox2 Is a Positive Timer of Oligodendrocyte

Development in the Postnatal Murine Spinal Cord. Mol. Neurobiol 55, 9001–9015. 10.1007/s12035-018-1035-7. [PubMed: 29623612]

16. Zhang S, Kim B, Zhu X, Gui X, Wang Y, Lan Z, Prabhu P, Fond K, Wang A, and Guo F (2020). Glial type specific regulation of CNS angiogenesis by HIFalpha-activated different signaling pathways. Nat. Commun 11, 2027. 10.1038/s41467-020-15656-4. [PubMed: 32332719]
17. Kuhlbrodt K, Herbarth B, Sock E, Hermans-Borgmeyer I, and Wegner M (1998). Sox10, a novel transcriptional modulator in glial cells. J. Neurosci 18, 237–250. 10.1523/JNEUROSCI.18-01-00237.1998. [PubMed: 9412504]
18. Ludwig A, Schlierf B, Schardt A, Nave KA, and Wegner M (2004). Sox10-rtTA mouse line for tetracycline-inducible expression of transgenes in neural crest cells and oligodendrocytes. Genesis 40, 171–175. 10.1002/gene.20083. [PubMed: 15493017]
19. Shibata S, Yasuda A, Renault-Mihara F, Suyama S, Katoh H, Inoue T, Inoue YU, Nagoshi N, Sato M, Nakamura M, et al. (2010). Sox10-Venus mice: a new tool for real-time labeling of neural crest lineage cells and oligodendrocytes. Mol. Brain 3, 31. 10.1186/1756-6606-3-31. [PubMed: 21034515]
20. Simon C, Lickert H, Gotz M, and Dimou L (2012). Sox10-iCreERT2 : a mouse line to inducibly trace the neural crest and oligodendrocyte lineage. Genesis 50, 506–515. 10.1002/dvg.22003. [PubMed: 22173870]
21. Armulik A, Genove G, and Betsholtz C (2011). Pericytes: developmental, physiological, and pathological perspectives, problems, and promises. Dev. Cell 21, 193–215. 10.1016/j.devcel.2011.07.001. [PubMed: 21839917]
22. Mazzoni J, Smith JR, Shahriar S, Cutforth T, Ceja B, and Agalliu D (2017). The Wnt Inhibitor Apcdd1 Coordinates Vascular Remodeling and Barrier Maturation of Retinal Blood Vessels. Neuron 96, 1055–1069 e1056. 10.1016/j.neuron.2017.10.025. [PubMed: 29154126]
23. Yu QC, Geng A, Preusch CB, Chen Y, Peng G, Xu Y, Jia Y, Miao Y, Xue H, Gao D, et al. (2022). Activation of Wnt/beta-catenin signaling by Zeb1 in endothelial progenitors induces vascular quiescence entry. Cell Rep. 41, 111694. 10.1016/j.celrep.2022.111694. [PubMed: 36417861]
24. Song S, Huang H, Guan X, Fiesler V, Bhuiyan MIH, Liu R, Jalali S, Hasan MN, Tai AK, Chattopadhyay A, et al. (2021). Activation of endothelial Wnt/beta-catenin signaling by protective astrocytes repairs BBB damage in ischemic stroke. Prog. Neurobiol 199, 101963. 10.1016/j.pneurobio.2020.101963. [PubMed: 33249091]
25. Langen UH, Ayloo S, and Gu C (2019). Development and Cell Biology of the Blood-Brain Barrier. Annu. Rev. Cell Dev. Biol 35, 591–613. 10.1146/annurev-cellbio-100617-062608. [PubMed: 31299172]
26. Knowland D, Arac A, Sekiguchi KJ, Hsu M, Lutz SE, Perrino J, Steinberg GK, Barres BA, Nimmerjahn A, and Agalliu D (2014). Stepwise recruitment of transcellular and paracellular pathways underlies blood-brain barrier breakdown in stroke. Neuron 82, 603–617. 10.1016/j.neuron.2014.03.003. [PubMed: 24746419]
27. Ayloo S, and Gu C (2019). Transcytosis at the blood-brain barrier. Curr. Opin. Neurobiol 57, 32–38. 10.1016/j.conb.2018.12.014. [PubMed: 30708291]
28. Ben-Zvi A, Lacoste B, Kur E, Andreone BJ, Mayshar Y, Yan H, and Gu C (2014). Mfsd2a is critical for the formation and function of the blood-brain barrier. Nature 509, 507–511. 10.1038/nature13324. [PubMed: 24828040]
29. Fernandez-Castaneda A, and Gaultier A (2016). Adult oligodendrocyte progenitor cells - Multifaceted regulators of the CNS in health and disease. Brain Behav. Immun 57, 1–7. 10.1016/j.bbi.2016.01.005. [PubMed: 26796621]
30. Nishiyama A, Shimizu T, Sherafat A, and Richardson WD (2021). Life-long oligodendrocyte development and plasticity. Semin. Cell Dev. Biol 116, 25–37. 10.1016/j.semcdb.2021.02.004. [PubMed: 33741250]
31. Seo JH, Maki T, Maeda M, Miyamoto N, Liang AC, Hayakawa K, Pham LD, Suwa F, Taguchi A, Matsuyama T, et al. (2014). Oligodendrocyte precursor cells support blood-brain barrier integrity via TGF-beta signaling. PloS One 9, e103174. 10.1371/journal.pone.0103174. [PubMed: 25078775]

32. Kimura I, Dohgu S, Takata F, Matsumoto J, Watanabe T, Iwao T, Yamauchi A, and Kataoka Y (2020). Oligodendrocytes upregulate blood-brain barrier function through mechanisms other than the PDGF-BB/PDGFRα pathway in the barrier-tightening effect of oligodendrocyte progenitor cells. Neurosci. Lett 715, 134594. 10.1016/j.neulet.2019.134594. [PubMed: 31678431]
33. Wang L, Geng J, Qu M, Yuan F, Wang Y, Pan J, Li Y, Ma Y, Zhou P, Zhang Z, and Yang GY (2020). Oligodendrocyte precursor cells transplantation protects blood-brain barrier in a mouse model of brain ischemia via Wnt/β-catenin signaling. Cell Death Dis. 11, 9. 10.1038/s41419-019-2206-9. [PubMed: 31907363]
34. Mayes DA, Rizvi TA, Titus-Mitchell H, Oberst R, Ciraolo GM, Vorhees CV, Robinson AP, Miller SD, Cancelas JA, Stemmer-Rachamimov AO, and Ratner N (2013). Nf1 loss and Ras hyperactivation in oligodendrocytes induce NOS-driven defects in myelin and vasculature. Cell Rep. 4, 1197–1212. 10.1016/j.celrep.2013.08.011. [PubMed: 24035394]
35. Tsai HH, Niu J, Munji R, Davalos D, Chang J, Zhang H, Tien AC, Kuo CJ, Chan JR, Daneman R, and Fancy SP (2016). Oligodendrocyte precursors migrate along vasculature in the developing nervous system. Science 351, 379–384. 10.1126/science.aad3839. [PubMed: 26798014]
36. Kang M, and Yao Y (2022). Laminin regulates oligodendrocyte development and myelination. Glia 70, 414–429. 10.1002/glia.24117. [PubMed: 34773273]
37. Yao Y (2017). Laminin: loss-of-function studies. Cell. Mol. Life Sci 74, 1095–1115. 10.1007/s00018-016-2381-0. [PubMed: 27696112]
38. Wang D, Wu F, Yuan H, Wang A, Kang GJ, Truong T, Chen L, McCallion AS, Gong X, and Li S (2017). Sox10(+) Cells Contribute to Vascular Development in Multiple Organs-Brief Report. Arterioscler. Thromb. Vasc. Biol 37, 1727–1731. 10.1161/ATVBAHA.117.309774. [PubMed: 28751573]
39. Stine ZE, Huynh JL, Loftus SK, Gorkin DU, Salmasi AH, Novak T, Purves T, Miller RA, Antonellis A, Gearhart JP, et al. (2009). Oligodendroglial and pan-neural crest expression of Cre recombinase directed by Sox10 enhancer. Genesis 47, 765–770. 10.1002/dvg.20559. [PubMed: 19830815]
40. Pingault V, Zerad L, Bertani-Torres W, and Bondurand N (2022). SOX10: 20 years of phenotypic plurality and current understanding of its developmental function. J. Med. Genet 59, 105–114. 10.1136/jmedgenet-2021-108105. [PubMed: 34667088]
41. Yao Y, Chen ZL, Norris EH, and Strickland S (2014). Astrocytic laminin regulates pericyte differentiation and maintains blood brain barrier integrity. Nat. Commun 5, 3413. 10.1038/ncomms4413. [PubMed: 24583950]
42. Chen ZL, and Strickland S (2003). Laminin gamma1 is critical for Schwann cell differentiation, axon myelination, and regeneration in the peripheral nerve. J. Cell Biol 163, 889–899. 10.1083/jcb.200307068. [PubMed: 14638863]
43. Rurak GM, Simard S, Freitas-Andrade M, Lacoste B, Charih F, Van Geel A, Stead J, Woodside B, Green JR, Coppola G, and Salmaso N (2022). Sex differences in developmental patterns of neocortical astroglia: A mouse translatome database. Cell Rep. 38, 110310. 10.1016/j.celrep.2022.110310. [PubMed: 35108542]
44. Li W, Berlinicke C, Huang Y, Giera S, McGrath AG, Fang W, Chen C, Takaesu F, Chang X, Duan Y, et al. (2023). High-throughput screening for myelination promoting compounds using human stem cell-derived oligodendrocyte progenitor cells. iScience 26, 106156. 10.1016/j.isci.2023.106156. [PubMed: 36852281]
45. Dincman TA, Beare JE, Ohri SS, and Whittemore SR (2012). Isolation of cortical mouse oligodendrocyte precursor cells. J. Neurosci. Methods 209, 219–226. 10.1016/j.jneumeth.2012.06.017. [PubMed: 22743801]
46. Zudaire E, Gambardella L, Kurcz C, and Vermeren S (2011). A computational tool for quantitative analysis of vascular networks. PloS One 6, e27385. 10.1371/journal.pone.0027385. [PubMed: 22110636]
47. Gautam J, Zhang X, and Yao Y (2016). The role of pericytic laminin in blood brain barrier integrity maintenance. Sci. Rep 6, 36450. 10.1038/srep36450. [PubMed: 27808256]

48. Sadeghian H, Lacoste B, Qin T, Toussay X, Rosa R, Oka F, Chung DY, Takizawa T, Gu C, and Ayata C (2018). Spreading depolarizations trigger caveolin-1-dependent endothelial transcytosis. Ann. Neurol 84, 409–423. 10.1002/ana.25298. [PubMed: 30014540]

49. Freitas-Andrade M, Comin CH, Van Dyken P, Ouellette J, Raman-Nair J, Blakeley N, Liu QY, Leclerc S, Pan Y, Liu Z, et al. (2023). Astroglial Hmgb1 regulates postnatal astrocyte morphogenesis and cerebrovascular maturation. Nat. Commun 14, 4965. 10.1038/s41467-023-40682-3. [PubMed: 37587100]

50. Rajani RM, Dupré N, Domenga-Denier V, Van Niel G, Heiligenstein X, and Joutel A (2021). Characterisation of early ultrastructural changes in the cerebral white matter of CADASIL small vessel disease using high-pressure freezing/freeze-substitution. Neuropathol. Appl. Neurobiol 47, 694–704. 10.1111/nan.12697. [PubMed: 33483954]

Main Points:

OL-derived laminin-γ1 actively regulates blood-brain barrier integrity and oligodendrocyte biology.

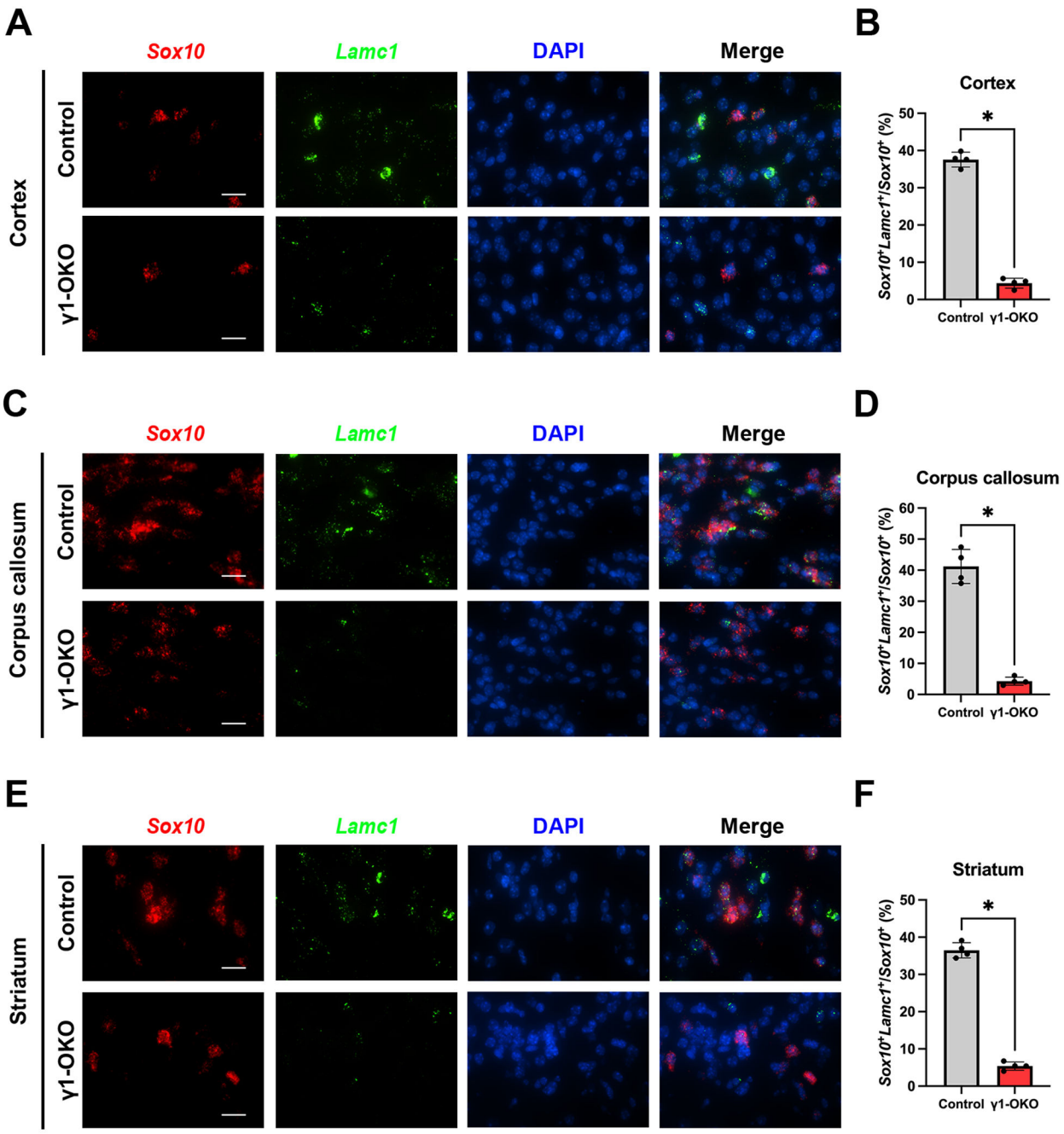

Figure 1. Laminin-γ1 is successfully deleted in OL lineage cells in γ1-OKO mice.

(A-F) Significant decreases in the percentages of *Sox10*$^+$*Lamc1*$^+$ cells/*Sox10*$^+$ cells were found in the cortex (A and B), corpus callosum (C and D), and striatum (E and F) of γ1-OKO mice compared to the controls. *p < 0.05, Mann-Whitney test. *n* = 4 mice. Scale bars: 20 μm.

Data were shown as mean ± SD.

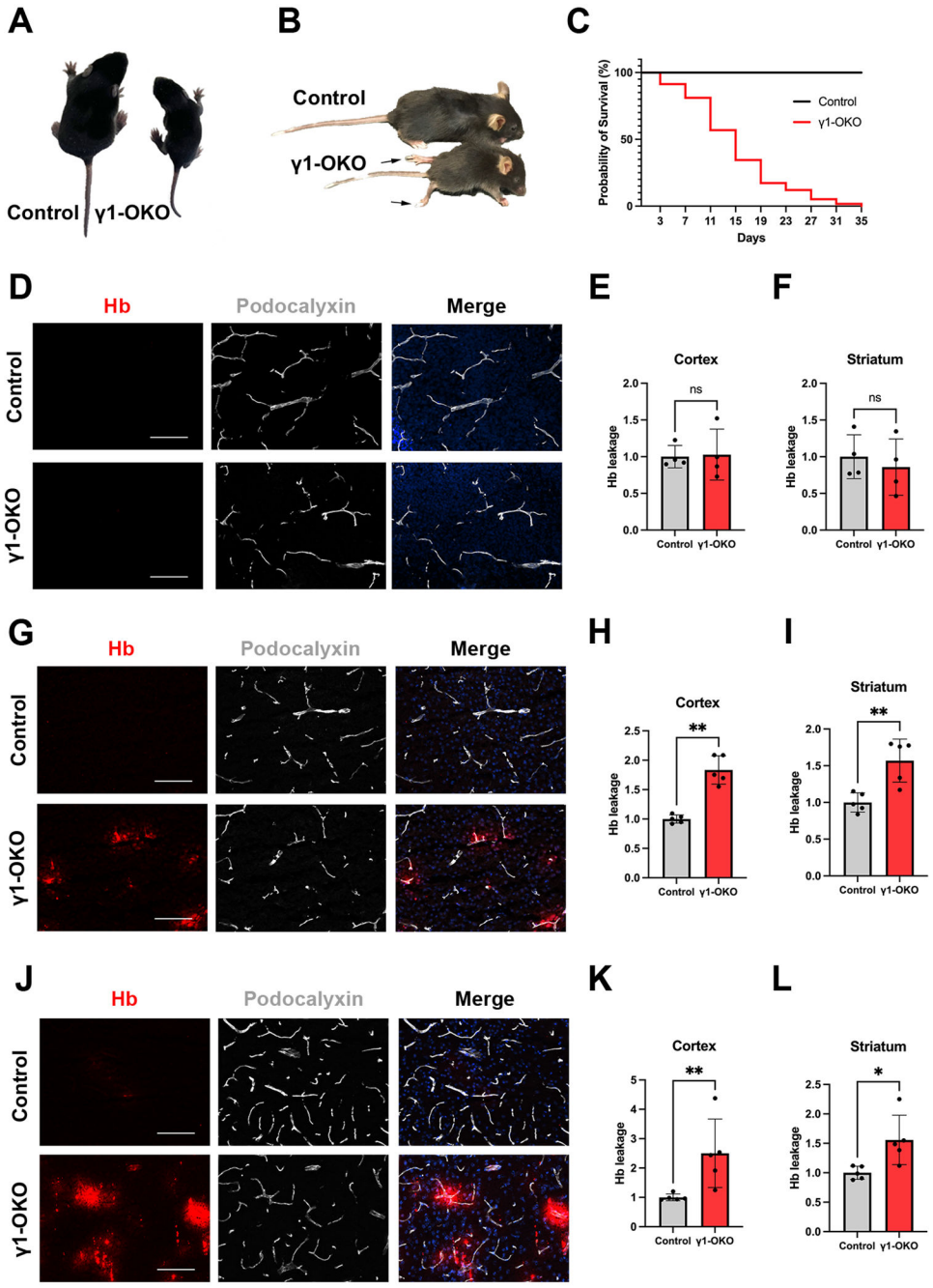

Figure 2. γ1-OKO mice exhibit muscle weakness and severe BBB disruption.

(A) γ1-OKO mice are smaller compared to their littermate controls at P8.

(B) By P28, γ1-OKO mice remain smaller and exhibit near-complete hindlimb paralysis.

(C) Survival plot of control (black) and γ1-OKO (red) mice.

(D) Representative images of hemoglobin (Hb) leakage in controls and γ1-OKO brains at P1. Scale bars: 100 μm.

(E-F) No changes in Hb levels were found in cortex (E) or striatum (F) of γ1-OKO mice at P1. ns; not significant, Mann-Whitney test. $n = 4$ mice.

(G) Representative images of Hb leakage in controls and γ1-OKO brains at P8. Scale bars: 100 μm.

(H-I) Significantly increased Hb levels were found in both cortex (H) and striatum (I) of γ1-OKO mice at P8. **p < 0.01, Mann-Whitney test. *n* = 5 mice.

(J) Representative images of Hb leakage in controls and γ1-OKO brains at P28. Scale bars: 100 μm.

(K-L) Significantly increased Hb levels were found in both cortex (K) and striatum (L) of γ1-OKO mice at P28. *p < 0.05, **p<0.01, Mann-Whitney test. *n* = 5 mice. Data were shown as mean ± SD.

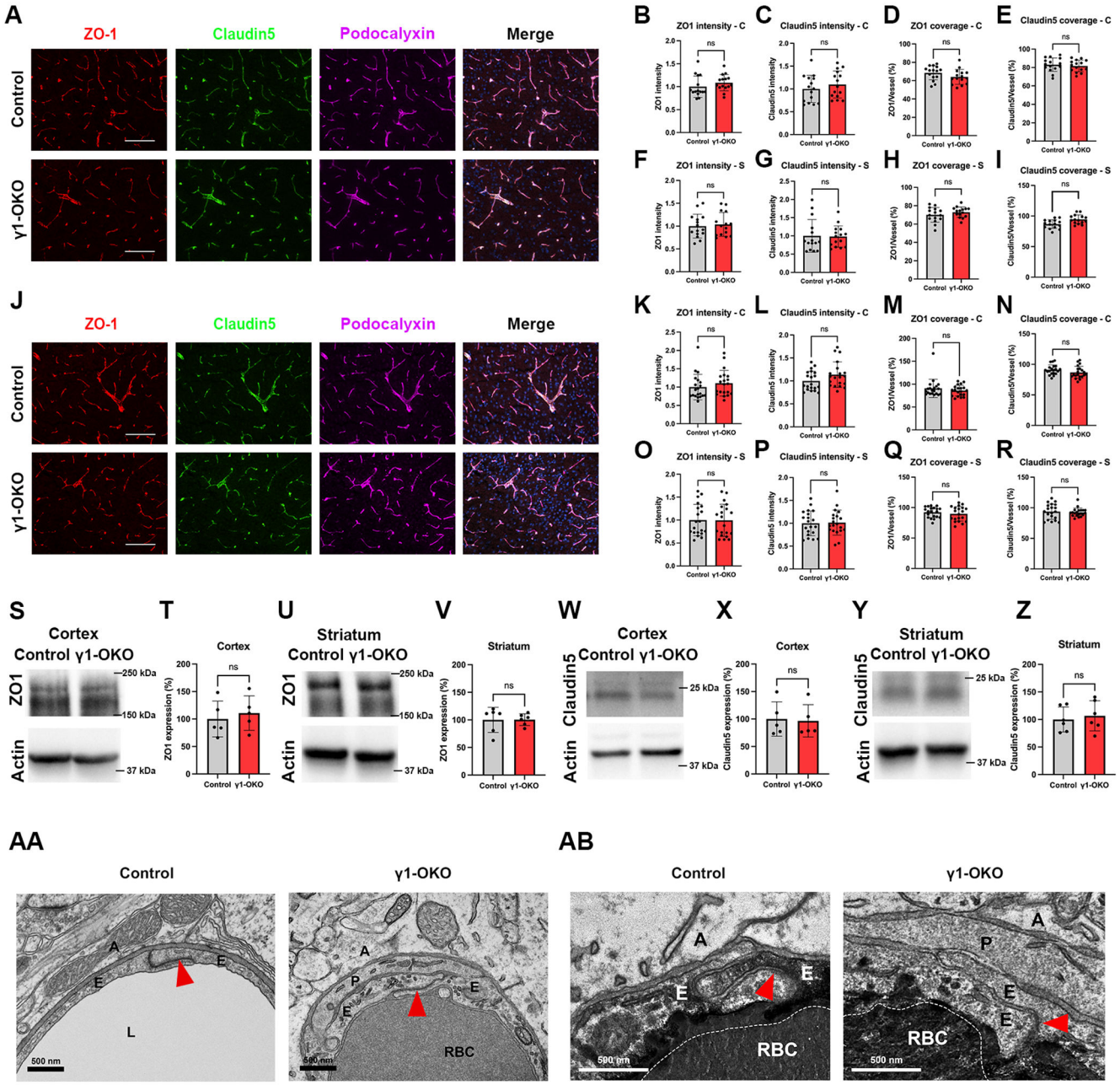

Figure 3. Tight junction is intact in γ1-OKO mice.

(A) Representative images of ZO-1/claudin5 and podocalyxin (vascular marker) staining in control and γ1-OKO brains at P15-17. Scale bars: 100 μm.

(B-I) Quantifications showing comparable ZO-1/claudin5 intensity and coverage between control and γ1-OKO mice at P15-17. ns; not significant, Mann-Whitney test. $n = 15$ sections from 3 mice.

(J) Representative images of ZO-1/claudin5 and podocalyxin staining in control and γ1-OKO brains at P28. Scale bars: 100 μm.

(K-R) Quantifications showing comparable ZO-1/claudin5 intensity and coverage between control and γ1-OKO mice at P28. ns; not significant, Mann-Whitney test. n = 20 sections from 4 mice.

(S-Z) Representative western blotting images and quantifications of ZO1 (S-V) and claudin5 (W-Z) expression in the cortex and striatum of control and γ1-OKO brains at P15-17. ns; not significant, Mann-Whitney test. n = 5-6 mice.

(AA) Representative TEM images showing intact tight junction structure in control and γ1-OKO mice at P15-17. Red arrowheads indicate tight junctions. Scale bars: 500 nm.

(AB) Representative TEM images showing that tight junctions prevented the leakage of HRP from the lumen in both control and γ1-OKO mice at P15-17. Red arrowheads indicate tight junctions. Scale bars: 500 nm.

Data were shown as mean ± SD. C; cortex, S; striatum, L; lumen, E; endothelial cell, P; pericyte, A; astrocyte, RBC; red blood cell.

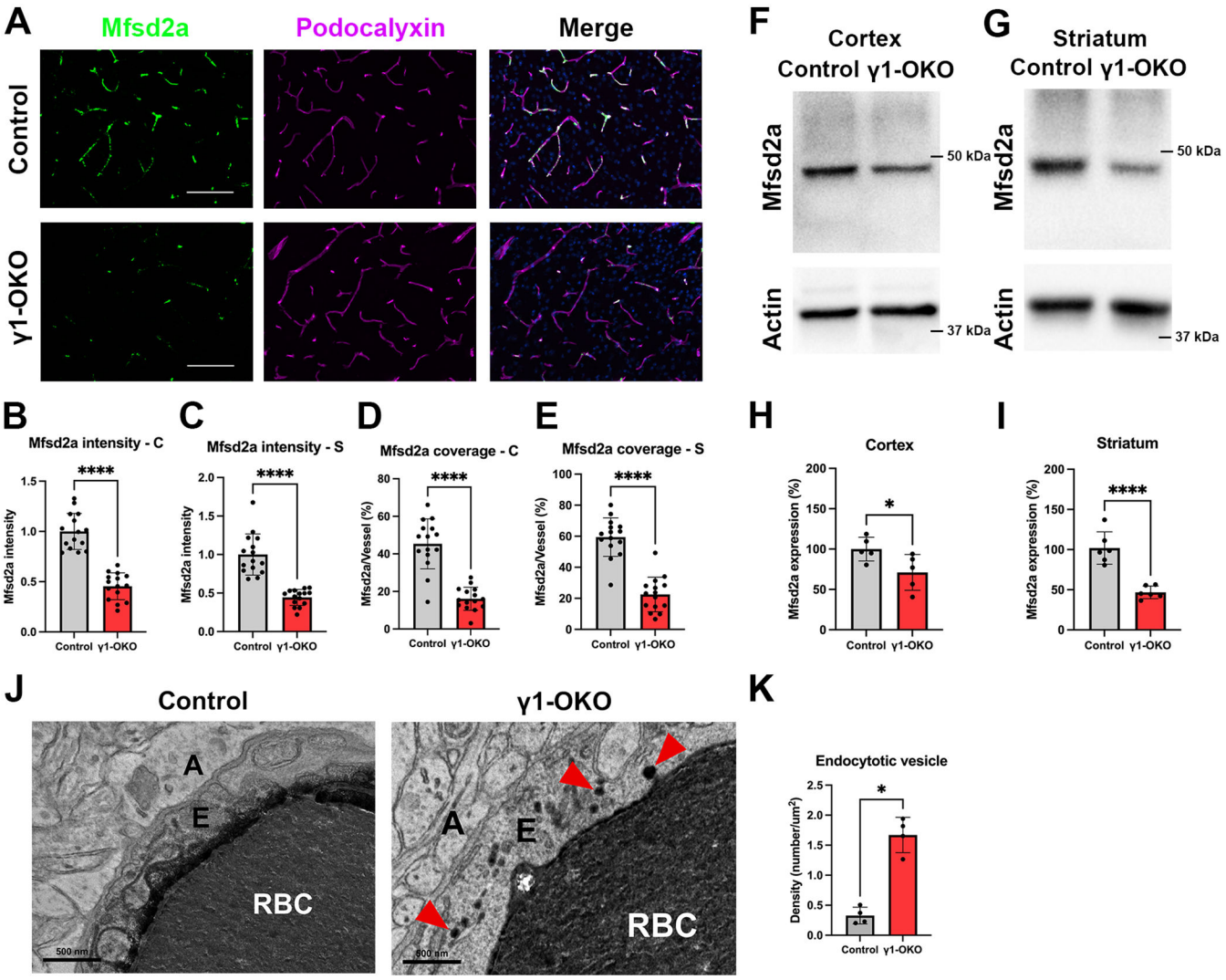

Figure 4. Transcellular transport is increased in γ1-OKO mice.

(A) Representative images of Mfsd2a and podocalyxin (vascular marker) staining in controls and γ1-OKO brains at P28. Scale bars: 100 μm.

(B-E) Quantifications showing significantly decreased Mfsd2a intensity (B and C) and coverage (D and E) in the cortex (B and D) and striatum (C and E) of γ1-OKO mice at P28. ****p < 0.0001, Mann-Whitney test. n = 15 sections from 3 mice.

(F-I) Representative western blotting images (F and G) and quantifications (H and I) of Mfsd2a expression in the cortex (F and H) and striatum (G and I) of control and γ1-OKO brains at P15-17. *p < 0.05, ****p<0.0001, Mann-Whitney test. n = 5-6 mice.

(J) Representative TEM images showing increased transcellular transport in γ1-OKO mice at P15-17. Arrowheads indicate HRP-filled transcytotic vesicles. Scale bars: 500 nm.

(K) Quantification showing significantly increased transcytotic vesicle density in γ1-OKO mice. *p < 0.05, Mann-Whitney test. n = 4 mice.

Data were shown as mean ± SD. E; endothelial cell, A; astrocyte, RBC; red blood cell.

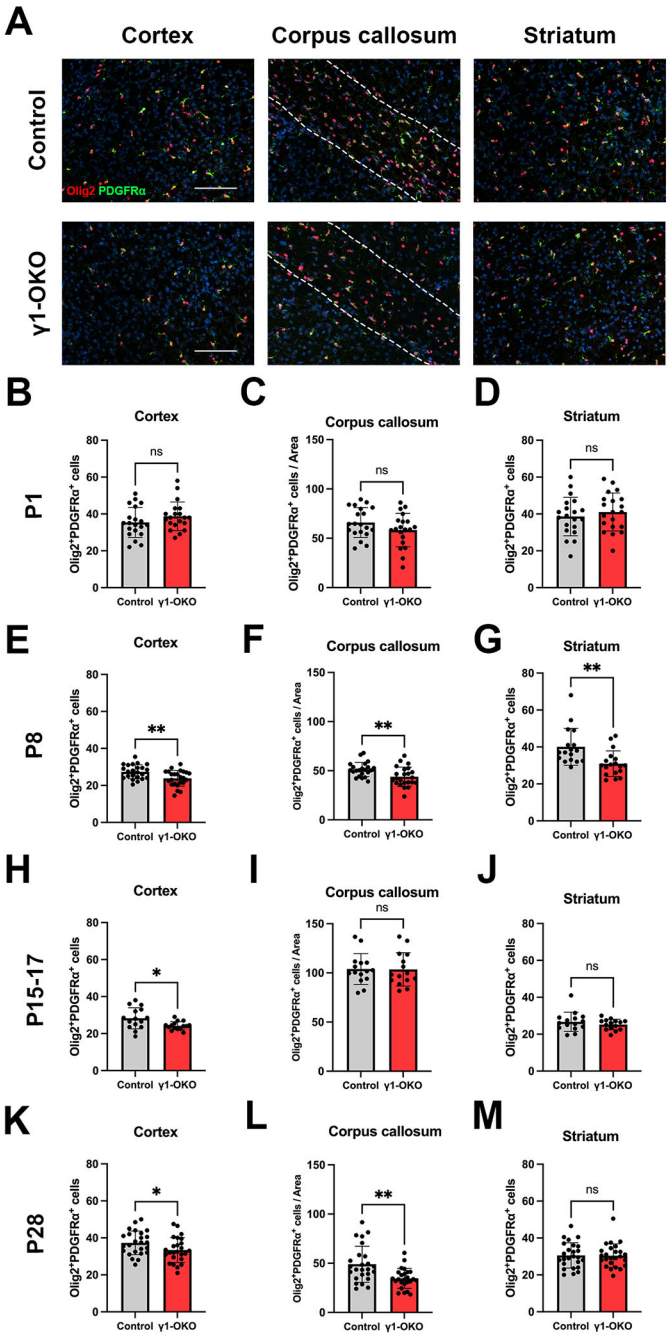

Figure 5. OPCs are decreased in γ1-OKO mice.

(A) Representative images of Olig2 and PDGFRα staining in the cortex, corpus callosum, and striatum of control and γ1-OKO mice at P8. Scale bars: 100 μm.

(B-M) Quantifications of OPC numbers in the cortex (B, E, H, and K), corpus callosum (C, F, I, and L), and striatum (D, G, J, and M) of control and γ1-OKO mice at P1 (B-D), P8 (E-G), P15-17 (H-J), and P28 (K-M). ns; not significant, *p < 0.05, **p < 0.01, Mann-Whitney test. *n* = 15-25 sections from 3-5 mice.

Data were shown as mean ± SD.

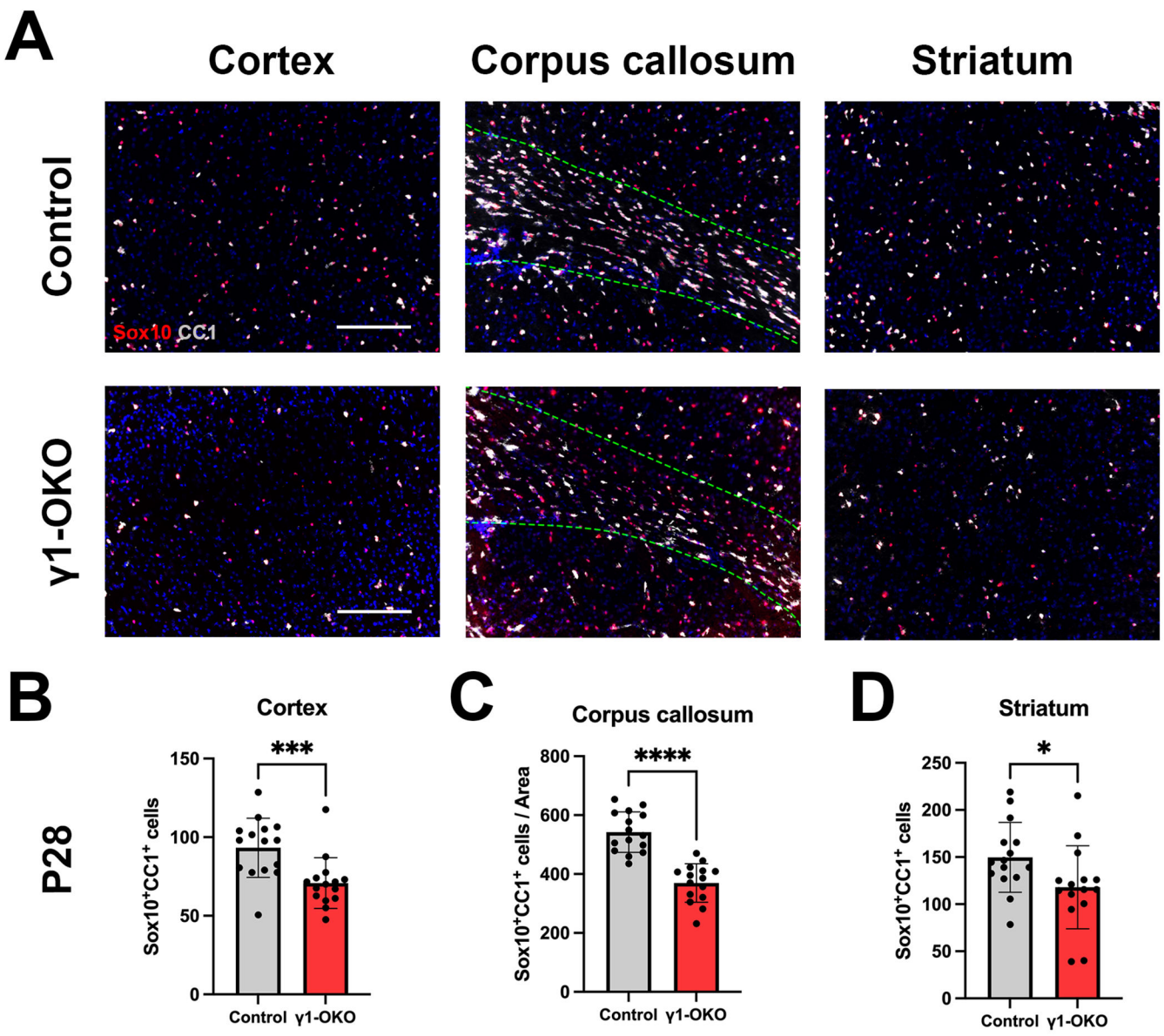

Figure 6. Mature-OLs are decreased in γ1-OKO mice.

(A) Representative images of Sox10 and CC1 staining in the cortex, corpus callosum, and striatum of control and γ1-OKO brains at P28. Scale bars: 100 μm.

(B-D) Quantifications of mature-OL numbers in the cortex (B), corpus callosum (C), and striatum (D) of control and γ1-OKO mice at P28. *p < 0.05, ***p < 0.001, ****p < 0.0001, Mann-Whitney test. *n* = 15 sections from 3 mice.

Data were shown as mean ± SD.

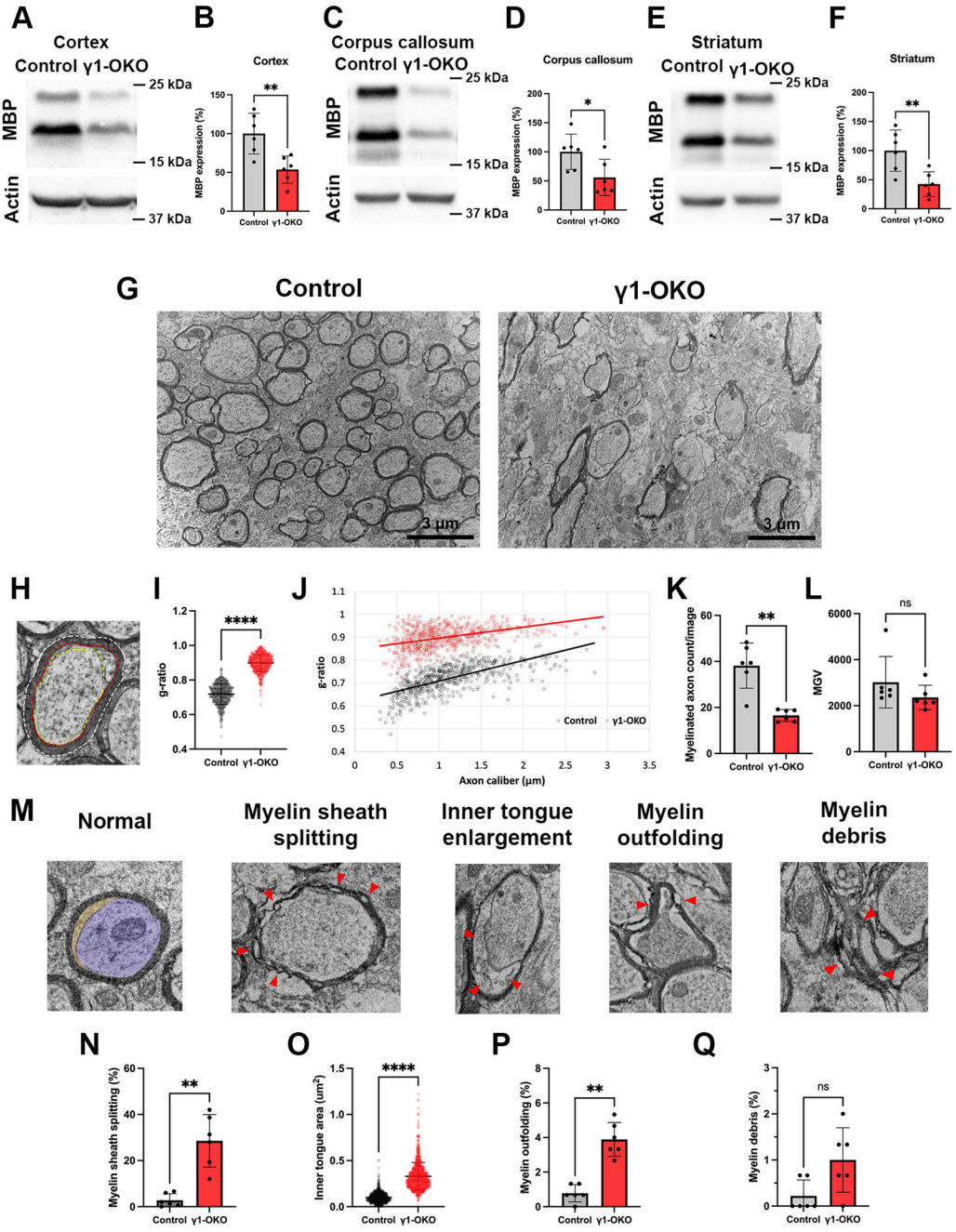

Figure 7. Myelination is impaired in γ1-OKO mice.

(A-F) Representative western blotting images and quantifications of MBP expression in the cortex (A-B), corpus callosum (C-D), and striatum (E-F) of control and γ1-OKO mice at P15-17. *p < 0.05, **p < 0.01, Mann-Whitney test. *n* = 6 mice.

(G) Representative TEM images of callosal myelinated fibers in the corpus callosum of control and γ1-OKO mice at P15-17. Scale bars: 3 μm.

(H) Illustration of various parameters used to calculate g-ratio. White, red, and yellow lines indicate the areas of myelinated fiber, axon + inner tongue, and axon, respectively.

(I) Quantification of g-ratio in control and γ1-OKO mice at P15-17. ****p < 0.0001, *t*-test. *n* = 617 (control) and 620 (γ1-OKO) values from 4 mice.
(J) Scatter plot of g-ratio against axon caliber indicating an upshift of g-ratio in γ1-OKO mice. *n* = 617 (control) and 620 (γ1-OKO) values from 4 mice.
(K) Quantification of myelinated fiber density in control and γ1-OKO mice at P15-17. **p < 0.01, Mann-Whitney test. *n* = 6 mice.
(L) Quantification of mean gray value (MGV) of compacted myelin sheaths in control and γ1-OKO mice at P15-17. ns; not significant, Mann-Whitney test. *n* = 6 mice.
(M) Representative TEM images showing normal and different types of abnormal morphology of myelin sheaths.
(N-Q) Quantifications of morphological abnormalities of myelin sheaths in control and γ1-OKO mice at P15-17. ns; not significant, **p < 0.01, ****p < 0.0001, Mann-Whitney test (N, P, and Q) and *t*-test (O). *n* = 6 mice (N, P, and Q), *n* = 920 (control) and 934 (γ1-OKO) values from 6 mice (O).
Data were shown as mean ± SD.

KEY RESOURCE TABLE

REAGENT or RESOURCE	SOURCE	IDENTIFIER
Antibodies		
Rabbit anti-hemoglobin	Cloud-Clone	Cat#PAB409Mu01
Goat anti-podocalyxin	R&D	Cat#AF1556; RRID:AB_354858
Rabbit anti-ZO1	ThermoFisher	Cat#61-7300; RRID:AB_2533938
Mouse anti-claudin5	Invitrogen	Cat#35-2500; RRID:AB_2533200
Rabbit anti-Mfsd2a	Dr. Chenghua Gu Lab	N/A
Rabbit anti-Olig2	Novus	Cat#NBP1-28667; RRID:AB_1914109
Goat anti-PDGFRα	R&D	Cat#AF2535; RRID:AB_2063012
Goat anti-Sox10	R&D	Cat#AF2864-SP; RRID:AB_442208
Mouse anti-CC1	Calbiochem	Cat#OP80; RRID:AB_2057371
Rat anti-MBP	BioRad	Cat#MCA409S; RRID:AB_325004
Rabbit anti-PDGFRβ	Cell Signaling	Cat#3169S
Mouse anti-SMA-Cy3	Sigma	Cat#C6198; RRID:AB_476856
Mouse anti-SMA-FITC	Sigma	Cat#F3777; RRID:AB_476977
Rabbit anti-Lef1	Cell Signaling	Cat#2230S
Goat anti-Sox17	R&D	Cat#AF1924; RRID:AB_355060
Rat anti-CD31	BD	Cat#553370; RRID:AB_394816
Rabbit anti-Ki67	GeneTex	Cat#GTX16667; RRID:AB_422351
Mouse anti-Olig2	Millipore	Cat#MABN50; RRID:AB_10807410
Rat anti-laminin-γ1	NeoMarkers	Cat#RT-795-P; RRID:AB_145593
Mouse anti-β-actin	BD	Cat#612657; RRID:AB_399901
Ultra-LEAF™ Purified anti-mouse CD16/32 antibody	Biolegend	Cat#101330
Anti-O4 MicroBeads	Miltenyi Biotec	Cat#130-096-670
Alexa Fluor-594 conjugated donkey anti-rabbit	Invitrogen	Cat#A21207; RRID:AB_141637
Alexa Fluor-488 conjugated donkey anti-rabbit	Invitrogen	Cat#A21206; RRID:AB_2535792
Alexa Fluor-647 conjugated donkey anti-rabbit	Invitrogen	Cat#A32795; RRID:AB_2762835
Alexa Fluor-647 conjugated donkey anti-goat	Invitrogen	Cat#A21447; RRID:AB_141844
Alexa Fluor-488 conjugated donkey anti-goat	Invitrogen	Cat#A11055; RRID:AB_2534102
Alexa Fluor-555 conjugated donkey anti-goat	Invitrogen	Cat#A21432; RRID:AB_2535853
Alexa Fluor-488 conjugated donkey anti-mouse	Invitrogen	Cat#A11001; RRID:AB_2534069
Alexa Fluor-647 conjugated donkey anti-mouse	Invitrogen	Cat#A31571; RRID:AB_162542
Alexa Fluor-488 conjugated donkey anti-rat	Invitrogen	Cat#A21208; RRID:AB_2535794
Alexa Fluor-647 conjugated goat anti-rat	Invitrogen	Cat#A21247; RRID:AB_141778
Chemicals, peptides, and recombinant proteins		
4kD FITC-Dextran	Sigma	Cat#FD4
HRP Type II	Sigma	Cat#P8250-25KU
Papain vial	Worthington Biochemical Corporation	Cat#LK003178

REAGENT or RESOURCE	SOURCE	IDENTIFIER
EBSS	Alfa Aesar	Cat#J67849
DNase I	Worthington Biochemical Corporation	Cat#LS002007
Albumin-ovomucoid inhibitor vial	Worthington Biochemical Corporation	Cat#LK003182
DPBS	Gibco	Cat#14190-136
DMEM	Gibco	Cat#11995-065
BSA	Sigma	Cat#A9647
Apo-transferrin	Sigma	Cat#T1147-100MG
Insulin	Sigma	Cat#I6634-50MG
Sodium selenite	Sigma	Cat#S5261-10G
D-biotin	Sigma	Cat#B4639-100MG
Hydrocortisone	Sigma	Cat#H0888-1G
PDGF-AA	R&D	Cat#221-AA-010
b-FGF	R&D	Cat#233-FB-010
PDL	Sigma	Cat#P7280-5MG
Critical commercial assays		
RNAscope in situ hybridization	Advanced Cell Diagnostics	Cat#323100
M.O.M.™ Kit	Vector Laboratories, Inc.	Cat#FMK-2201
BCA Protein Assay Kit	Pierce	Cat#23227
Clarity Max™ Western ECL Substrate	Bio-Rad	Cat#1705062
Deposited Data		
Raw data	This paper	https://digitalcommonsdata.usf.edu/datasets/jmszrtgd48/draft?a=14077a44-68de-4f5b-bcb7-40e5a304e4b3
Experimental models: Organisms/strains		
Mouse: B6.129P2-*Lamc1*^{tm1Strl}/J	The Jackson Laboratory	JAX: 016917
Mouse: B6;CBA-Tg(Sox10-cre)1Wdr/J	The Jackson Laboratory	JAX: 025807
Software and algorithms		
Angiotool	National Cancer Institute	https://ccrod.cancer.gov/confluence/display/ROB2/Home
ImageJ	NIH	https://imagej.nih.gov/ij/
GraphPad Prism 9	GraphPad	https://www.graphpad.com/features
Photoshop	Adobe	https://www.adobe.com